https://doi.org/10.70882/31jhh176

SCIENCE FORUM (JOURNAL OF PURE AND APPLIED SCIENCES) 26, (5 Special) (2026), 489 - 509

Science Forum (Journal of Pure and Applied Sciences)

Journal Homepage: https://atbuscienceforum.com.ng/index.php/jpas

Weighted Sobolev Estimates and Conditional Regularity for the Three-Dimensional Navier–Stokes Equations: Energy, Pressure, and Vorticity–Strain Identities

Bilal Ahmed Shihab

Holy Karbala Directorate General of Education, 56001, Karbala, Iraq

Abstract

We present weighted Sobolev and energy estimates for incompressible Navier-Stokes flow and distinguish strictly positive weights from truly degenerate weights. The larger norm-equivalence proof has been generalized and unweighted control is shown to fail in the degeneracy domain. We present a one-dimensional example of Muckenhoupt A2, which gives a quantitative degenerate Poincaré inequality. For a periodic Taylor-Green benchmark we obtain the second-order residual constant with the exact pressure and weighted energy corrections. Beyond the conventional checks, we adopt weighted and standard piecewise-linear Galerkin solvers for an invariant three-dimensional Navier-Stokes shear flow. Both schemes solve the same physical equation with Crank-Nicolson time integration. We prove a new, explicitly quantified discrete stability statement for this restricted shear approximation, derive the corresponding discrete energy identity and global error estimate with smoothness, and report the measured spatial and temporal estimates together with the correction of the weight gradients. Our calculations do not claim a weighted accuracy advantage or solve the open three-dimensional global regularity problem.

Keywords

Incompressible Navier–Stokes Equations;
Weighted Sobolev Spaces;
Energy Estimates;
Muckenhoupt Weights;
Pressure–Vorticity Coupling;
Conditional Regularity.

EISSN: 3156-5190 (Online)
ISSN: 1119-4618 (Print)
JPAS
Faculty of Science, ATBU Bauchi

Corresponding Author: Bilal Ahmed Shihab, Holy Karbala Directorate General of Education, 56001, Karbala, Iraq Bilal_ahmed@karbala.edu.iq

© 2026 Faculty of Science, ATBU Bauchi. All rights reserved

1. Introduction

The incompressible Navier-Stokes equations describe the motion of a viscous fluid and have been used in the mathematical study of shear, vorticity generation and transport. Global finite-energy weak solutions in three dimensions have been known since Leray's work and global smoothness and uniqueness for unrestricted smooth three-dimensional initial data remain open today [1-3]. Any theorem that is to settle the question has to provide estimates close to the unknown solution size, and a formal Galerkin construction does not do that.

Weighted Sobolev norms may be able to capture local spatial behavior such as interfaces and geometric features. Muckenhoupt weights are a natural analytic setting for weighted inequalities [4,5]. However, introducing a spatial weight into an energy functional does not automatically change the governing equations or give rise to an independent conservation principle. In particular, gradients of the weight generate additional terms when integrating by parts and these terms need to be estimated explicitly.

This study combines exact mathematical identities with two separate verification levels: the original periodic Taylor–Green finite-difference consistency audit, and a genuine finite-element weighted-versus-standard Galerkin time-integration experiment. The Taylor–Green tables test spatial operator truncation and diagnostic energy quadrature; the newly computed Galerkin tables test discrete stability, convergence and integrated energy. We derive a new restricted shear-subspace energy statement rather than asserting unrestricted three-dimensional regularity, and connect each table to its proven assertion [7,10–14].

In all that follows, a diagnostic multiplier does not enter the physical Navier–Stokes equation, whereas a weighted Galerkin test measure changes the finite-dimensional equations without changing the underlying continuum PDE. Density- or viscosity-weighted physical models would instead require a consistently modified momentum law. The three meanings of "weight" are kept distinct in every numerical table.

Throughout, $\Omega \subset \mathbb{R}^3$ is a bounded, connected domain with C^2 boundary, $\nu > 0$ is the kinematic viscosity, and $T > 0$. We consider

$$\partial_t u + (u \cdot \nabla)u - \nu\Delta u + \nabla p = f, \qquad \nabla \cdot u = 0 \quad \text{in } \Omega \times (0,T),$$

with $u|_{\partial\Omega} = 0$ and $u(\cdot,0) = u_0$. The density has been normalized to one. A weight w introduced below is an analytic multiplier, not automatically a physical variable-density coefficient.

The development of weighted estimates starts with Muckenhoupt's description of weights for the Hardy-Littlewood maximal operator [4]. The degenerate elliptic theory of Fabes, Kenig and Serapioni [5] shows that weights can replace the uniform ellipticity in some local regularity arguments, and in this way it does not lead to a weighted Stokes spectral theorem or three-dimensional global regularity. The classical Navier-Stokes existence, weak compactness and approximation are also developed systematically in Temam [7]. Fujita and Kato [10] give a fundamental local and small-data initial-value theory and Caffarelli, Kohn and Nirenberg [9] establish partial regularity and not unrestricted smoothness. These are the important features to make a weighted regularity case.

Galerkin discretization of incompressible flow requires a consistent treatment of velocity, pressure, incompressibility and the discrete energy mechanism; see Girault and Raviart [11]. Heywood and Rannacher [12] analyze spatial error for nonstationary Navier–Stokes flow under the necessary regularity assumptions, while their later work [13] treats second-order temporal discretization. Crank and Nicolson [14] introduced the implicit time-centering method used in the numerical experiment below. The present contribution specializes these established ideas to an explicitly weighted residual formulation, derives its coercivity threshold and discrete energy

identity, and compares two computations on exactly the same physical equation.

A **diagnostic weight** multiplies a norm or an integral evaluated *after* a velocity field has been computed. It cannot influence that field. A **numerical test weight** changes the trial/test projection (and hence the computed finite-dimensional approximation) while leaving the differential equation unchanged. A **physical coefficient**, such as density or viscosity, changes the governing model and must appear consistently in its mass, stress, and boundary terms. We use diagnostic weights in the Taylor–Green audit and numerical test weights in the Galerkin comparison; no experiment treats a diagnostic multiplier as a variable physical density.

2. Weighted functional setting and analytical results

Let $1 < \mathrm{p} < \infty$, and suppose $\mathrm{w}: \Omega \to (0, \infty)$ is measurable. The weighted Lebesgue and first-order Sobolev norms are

$$\| \mathrm{v} \|_{\mathrm{L}^{\mathrm{p}}_{\mathrm{w}}(\Omega)} = \left(\int_{\Omega} |\mathrm{v}|^{\mathrm{p}} \, \mathrm{w} \, \mathrm{dx} \right)^{1/\mathrm{p}}, \qquad \| \mathrm{v} \|_{\mathrm{W}^{1,\mathrm{p}}_{\mathrm{w}}(\Omega)} = \left(\int_{\Omega} (|\mathrm{v}|^{\mathrm{p}} + |\nabla \mathrm{v}|^{\mathrm{p}}) \, \mathrm{w} \, \mathrm{dx} \right)^{1/\mathrm{p}}.$$

The space $\mathrm{W}^{1,\mathrm{p}}_{\mathrm{w}}(\Omega)$ consists of functions for which the indicated weak derivatives are weighted p-integrable. For a general $\mathrm{A_p}$ weight, density, compact embeddings, boundary traces, and elliptic regularity require separate assumptions; they are not established by the norm definition alone. In the main results we adopt the explicit sufficient condition

$$0 < \mathrm{w}_* \le \mathrm{w}(\mathrm{x}) \le \mathrm{w}^* < \infty \quad \text{for a.e. } \mathrm{x} \in \Omega, \qquad \mathrm{w} \in \mathrm{W}^{1,\infty}(\Omega).$$

Condition (3) is stronger than $\mathrm{w} \in \mathrm{A_p}$ but has the advantage that every estimate used below is immediate and mathematically transparent. Indeed,

$$\mathrm{w}_*^{1/\mathrm{p}} \| \mathrm{v} \|_{\mathrm{W}^{1,\mathrm{p}}(\Omega)} \le \| \mathrm{v} \|_{\mathrm{W}^{1,\mathrm{p}}_{\mathrm{w}}(\Omega)} \le (\mathrm{w}^*)^{1/\mathrm{p}} \| \mathrm{v} \|_{\mathrm{W}^{1,\mathrm{p}}(\Omega)}.$$

Thus, under (3), weighted regularity and ordinary Sobolev regularity describe the same underlying function class, with different norm constants. A weight that degenerates or becomes singular may lead to a genuinely different function space, but extending the arguments to such a weight requires a separate weighted Stokes and compactness theory.

Muckenhoupt conditions and genuinely degenerate weights

For $1 < p < \infty$, a locally integrable positive weight belongs to A_p if

$$[w]_{A_p} = \sup_I \left(\frac{1}{|I|} \int_I w(y)\, dy \right) \left(\frac{1}{|I|} \int_I w(y)^{-1/(p-1)}\, dy \right)^{p-1} < \infty,$$

where the supremum runs over subintervals I of the domain. The bounded-weight hypothesis (3) implies $[w]_{A_p} \le w^*/w_*$, but the reverse implication is false: A_p includes weights that approach zero or become unbounded. In particular, the one-dimensional power weight $w_\beta(y) = y^\beta$ on $(0,1)$ belongs to A_2 precisely when $-1 < \beta < 1$; its characteristic is $[w_\beta]_{A_2} = 1/(1-\beta^2)$. This one-dimensional calculation must not be interpreted as an A_2-based existence theorem for the three-dimensional weighted Stokes operator [4,5].

Lemma 2 (quantitative degenerate Dirichlet estimate). If $-1 < \beta < 1$ and $v \in C_c^\infty(0,1)$, then

$$\int_0^1 y^\beta |v(y)|^2\, dy \le \frac{1}{1-\beta^2} \int_0^1 y^\beta |v'(y)|^2\, dy.$$

Proof. Using $v(1) = 0$ and Cauchy–Schwarz with reciprocal powers gives

$$|v(y)|^2 \le \left(\int_y^1 s^\beta\,|v'(s)|^2\,ds\right)\left(\int_y^1 s^{-\beta}\,ds\right) \le \frac{1}{1-\beta}\int_0^1 s^\beta\,|v'(s)|^2\,ds.$$

Multiplication by y^β and integration from zero to one produces the stated constant because $\int_0^1 y^\beta\,dy = (1+\beta)^{-1}$. Density gives the same estimate on the closure of C_c^∞ in the weighted norm. This proves the lemma without assuming $\inf w_\beta > 0$.

This is a separate **degenerate weighted estimate** and cannot be substituted into Theorem 1 to conclude unweighted H^1 regularity. Indeed, for a boundary-layer test $v_\varepsilon(y) = \eta(y/\varepsilon)$ supported in $(0,2\varepsilon)$, the quotient $\int w_\beta|v_\varepsilon'|^2/\int |v_\varepsilon'|^2$ is proportional to ε^β and tends to zero when $\beta > 0$. Thus no positive constant independent of v bounds the unweighted gradient by the weighted gradient. Moreover, the constant $(1-\beta^2)^{-1}$ blows up as $|\beta| \uparrow 1$. Uniformity holds only for $|\beta| \le 1-\delta$, where its value is at most $(2\delta-\delta^2)^{-1}$. Boundary traces, density, weighted pressure recovery and compactness must be checked separately for a full degenerate-flow theory.

Lemma 1 (Dirichlet weighted Poincaré inequality). Assume that Ω is bounded and Lipschitz and w satisfies the two-sided bounds in (3). For every $v \in W_0^{1,p}(\Omega)$,

$$\| v \|_{L^p_w(\Omega)} \le C_P \left(\frac{w^*}{w_*}\right)^{1/p} \| \nabla v \|_{L^p_w(\Omega)},$$

where C_P is the ordinary unweighted Dirichlet Poincaré constant.

Proof. Apply the upper weight bound, the classical Poincaré inequality, and then the lower weight bound:

$$\int_\Omega |v|^p\,w\,dx \le w^*\,\| v \|_{L^p}^p \le w^* C_P^p\,\| \nabla v \|_{L^p}^p \le \frac{w^* C_P^p}{w_*}\int_\Omega |\nabla v|^p\,w\,dx.$$

Taking pth roots prove (5). ▫

For the weighted-mean-zero Neumann formulation, the weighted mean $\mathrm{v_w} = \left(\int_\Omega \mathrm{v\,w\,dx}\right)/\left(\int_\Omega \mathrm{w\ dx}\right)$ must be used, and the corresponding argument involves the mean-zero Poincaré theorem. The hypotheses for that formulation should not be silently substituted for the Dirichlet assumptions above.

Exact weighted energy balance

We assume for the derivation that (u, p) is smooth enough to justify integration by parts. Write

$$\mathrm{E_w(t)} = \frac{1}{2}\int_\Omega \mathrm{w}\,|\mathrm{u(x,t)}|^2\,\mathrm{dx}, \qquad \mathrm{D_w(t)} = \int_\Omega \mathrm{w}\,|\nabla \mathrm{u(x,t)}|^2\,\mathrm{dx}.$$

Proposition 1 (weighted energy identity). For a time-independent weight satisfying (3) and no-slip boundary conditions, the solution of (1) obeys

$$\frac{dE_w}{dt} + \nu D_w = \int_\Omega w\,\mathbf{f}\cdot\mathbf{u}\,dx + \frac{1}{2}\int_\Omega |\mathbf{u}|^2\,\mathbf{u}\cdot\nabla w\,dx + \int_\Omega p\,\mathbf{u}\cdot\nabla w\,dx - \nu\int_\Omega (\nabla\mathbf{u})^{\mathrm{T}}\,\mathbf{u}\cdot\nabla w\,dx.$$

Proof. Multiply (1) by $w\mathbf{u}$ and integrate. The temporal term equals dE_w/dt. Incompressibility and the boundary condition give

$$\int_\Omega w\,\mathbf{u}\cdot(\mathbf{u}\cdot\nabla)\mathbf{u}\,dx = -\frac{1}{2}\int_\Omega |\mathbf{u}|^2\,\mathbf{u}\cdot\nabla w\,dx.$$

The pressure term is

$$\int_\Omega w\,\mathbf{u}\cdot\nabla p\,dx = -\int_\Omega p\,\mathbf{u}\cdot\nabla w\,dx,$$

and the viscous contribution satisfies

$$-\nu \int_{\Omega} w\,\mathbf{u}\cdot\Delta\mathbf{u}\,dx = \nu D_w + \nu \int_{\Omega} (\nabla\mathbf{u})^{\mathrm{T}}\,\mathbf{u}\cdot\nabla w\,dx.$$

Substitution proves (8). ▫

Identity (8) is the central quantitative correction to a naive weighted-energy argument. Unless $\nabla \mathrm{w} = 0$, nonlinear advection and pressure generally contribute to the rate of weighted energy; they cannot be discarded by incompressibility alone. For example, the last term admits the estimate

$$\nu\left|\int_{\Omega} (\nabla \mathrm{u})^{\mathrm{T}}\,\mathrm{u}\cdot\nabla \mathrm{w}\,\mathrm{dx}\right| \le \frac{\nu}{4}\mathrm{D_w} + \frac{\nu \parallel \nabla \mathrm{w} \parallel^2_{\mathrm{L}^\infty}}{\mathrm{w}_*^2}\int_{\Omega} \mathrm{w}\,|\mathrm{u}|^2\,\mathrm{dx}.$$

The displayed constant is a sufficient, not necessarily sharp, bound. Controlling the cubic term in (8) requires additional norms and interpolation; controlling the pressure term requires a pressure estimate and appropriate normalization. Therefore, (8) by itself is not a closed global H^1 bound for arbitrary three-dimensional data.

Setting $\mathrm{w} \equiv 1$ removes all three weight-gradient corrections:

$$\frac{1}{2}\frac{\mathrm{d}}{\mathrm{dt}} \parallel \mathrm{u} \parallel^2_{\mathrm{L}^2} + \nu \parallel \nabla \mathrm{u} \parallel^2_{\mathrm{L}^2} = (\mathrm{f}, \mathrm{u})_{\mathrm{L}^2}.$$

For Leray–Hopf weak solutions, this becomes an energy inequality for almost every initial time [1–3]. It is important to distinguish the viscous dissipation in (13) from the conservation of kinetic energy in inviscid ideal flow. Similarly, the fluid-mechanical mass balance for an incompressible constant-density flow should not be interpreted as an additional independent scalar conservation law generated by w.

Pressure–vorticity coupling in a weighted identity

Define vorticity by $\omega = \nabla \times \mathrm{u}$. Applying curl to the pointwise momentum equation gives

$$\partial_{\mathrm{t}}\omega + (\mathrm{u}\cdot\nabla)\omega = (\omega\cdot\nabla)\mathrm{u} + \nu\Delta\omega + \nabla\times \mathrm{f}.$$

The ordinary pressure gradient disappears because $\nabla \times \nabla \mathrm{p} = 0$. A weighted pressure gradient behaves differently:

$$\nabla \times (\mathrm{w}\nabla \mathrm{p}) = \nabla \mathrm{w} \times \nabla \mathrm{p}.$$

Proposition 2 (weighted curl identity). Under sufficient differentiability,

$$\nabla w \times \nabla p = \nabla \times (w\mathbf{f}) - \nabla \times (w\,\partial_t \mathbf{u}) - \nabla \times (w(\mathbf{u}\cdot\nabla)\mathbf{u}) + \nu\nabla \times (w\Delta\mathbf{u}).$$

Proof. Rearrange (1) to isolate ∇p; multiply by w; apply the linear curl operator and then (15). ▫

For a steady flow, $\partial_{\mathrm{t}}\mathrm{u} = 0$ in (16). The expression is a product-rule identity rather than a new commutation law: it does not assert that curl commutes with multiplication by a variable weight. The term $\nabla \mathrm{w} \times \nabla \mathrm{p}$ vanishes when w is constant or when $\nabla \mathrm{w}$ and $\nabla \mathrm{p}$ are parallel. These are testable conditions, not generic properties of incompressible flow.

Existence, uniqueness, and the limitations of weighted estimates

We distinguish weak solutions, local strong solutions, and global strong solutions. For data $\mathrm{u}_0 \in \mathrm{L}^2_\sigma(\Omega)$ and suitable forcing, global Leray–Hopf weak solutions are known to exist [1–3]. For sufficiently regular divergence-free initial data, standard three-dimensional local strong-solution theory yields existence and uniqueness on a possibly short time interval. Proving that such an interval always extends to infinite time for arbitrary smooth three-dimensional data remains unresolved.

Theorem 1 (equivalence of weighted and unweighted smallness under nondegenerate weights). Suppose (3) holds. Then for every divergence-free $u_0 \in H_0^1(\Omega)^3$,

$$\sqrt{w_*}\ \| u_0 \|_{H^1(\Omega)} \le \| u_0 \|_{H_w^1(\Omega)} \le \sqrt{w^*}\ \| u_0 \|_{H^1(\Omega)}.$$

Consequently, any established standard global strong-solution theorem whose hypothesis is a sufficiently small H^1 norm can be reformulated as a sufficient weighted smallness condition. Such reformulation does not enlarge the data class by itself.

Expanded proof of Theorem 1, with uniformity and degeneration. Write $m = \operatorname{ess\,inf}_\Omega w$ and $M = \operatorname{ess\,sup}_\Omega w$. For every scalar weak derivative $D^\alpha v$, with $|\alpha| \le 1$, the pointwise inequalities $m|D^\alpha v|^2 \le w|D^\alpha v|^2 \le M|D^\alpha v|^2$ hold almost everywhere. Integrating and summing over the three velocity components and all derivatives yields

$$m \| u_0 \|_{H^1}^2 \le \| u_0 \|_{H_w^1}^2 \le M \| u_0 \|_{H^1}^2.$$

The square-root inequalities prove the norm equivalence and show that the identity map between the two Hilbert spaces and its inverse have operator norms at most $\sqrt{M}$ and $m^{-1/2}$, respectively. These bounds depend on m, M, but **not** on time or on the finite-dimensional Galerkin dimension. Suppose a separately established strong-solution theorem, for specified boundary conditions and forcing, requires $\| u_0 \|_{H^1} \le \varepsilon_*$. Its weighted sufficient condition is $\| u_0 \|_{H_w^1} \le \sqrt{m}\,\varepsilon_*$. The converse weighted estimate only implies $\| u_0 \|_{H_w^1} \le \sqrt{M}\,\varepsilon_*$ from an unweighted-small datum. Neither statement changes the existence theory [7,10].

For a time-dependent family of weights w_t with the *same* bounds $0 < m \le w_t \le M$, these constants remain uniform in t; for a family w_ε with $m_\varepsilon \downarrow 0$, the inverse bound $m_\varepsilon^{-1/2}$ diverges, and Theorem 1 supplies no uniform continuation criterion. For instance, $w_\varepsilon(y) = \varepsilon + y^\beta$ with $0 < \beta < 1$ has $m_\varepsilon = \varepsilon$ and $\| u \|_{H^1} \le \varepsilon^{-1/2} \| u \|_{H_{w_\varepsilon}^1}$. The limiting weight is in A_2 in the one-dimensional model, but a uniform unweighted three-dimensional bound cannot be inferred. This identifies precisely where the nondegenerate proof stops.

Proposition 3 (conditional extension of a strong solution). Let $\mathbf{u}$ be a strong solution of (1) on $[0, T_*)$ in a standard function class admitting the usual local existence and continuation theorem, with compatible smooth boundary data and sufficiently regular forcing. If

$$\sup_{0 \le t < T_*} \| \mathbf{u}(t) \|_{H_w^1(\Omega)} < \infty$$

and the remaining regularity hypotheses of that continuation theorem hold, then the corresponding unweighted H^1 norm remains bounded; hence the same standard continuation criterion applies.

Justification. Inequality (4) gives $\| \mathbf{u}(t) \|_{H^1} \le w_*^{-1/2} \| \mathbf{u}(t) \|_{H_w^1}$. One may therefore apply the pre-existing continuation result to the unweighted solution. The essential open step would be proving (18) without assuming it. This conditional proposition does not provide that missing bound.

For a divergence-free Stokes basis $\{e_j\}$, a standard approximation is

$$u_m(x,t) = \sum_{j=1}^{m} a_j^{(m)}(t) e_j(x).$$

Deriving an m-independent $L^\infty(0,T;L^2) \cap L^2(0,T;H_0^1)$ estimate yields weak compactness and supports the classical weak-solution limit. Strong compactness in the spaces needed to control all nonlinear derivatives, and uniform higher regularity up to arbitrary T, require additional estimates. Simply introducing a basis described as "weighted Stokes eigenfunctions" does not prove that a suitable self-adjoint weighted Stokes operator exists; its domain, divergence constraint, boundary conditions, and spectral properties must be defined first.

Vorticity–strain interaction: evolution, not automatic conservation

Let the symmetric strain-rate tensor and the material derivative be

$$S = \frac{1}{2}(\nabla u + (\nabla u)^{T}), \qquad \frac{D}{Dt} = \partial_t + u \cdot \nabla.$$

Define the candidate weighted interaction functional

$$Q_w(t) = \int_{\Omega} w\,(x)\ \omega(x,t) \cdot S(x,t)\omega(x,t)\,dx.$$

This scalar measures a weighted interaction between vortex stretching and local deformation; because S need not be positive semidefinite, Q_w is not generally nonnegative. Its time derivative can be written exactly.

Proposition 4 (evolution identity). For a smooth solution with time-independent w and boundary conditions that remove the material-flux boundary integral,

$$\frac{dQ_w}{dt} = \int_{\Omega} w\left[2\left(\frac{D\boldsymbol{\omega}}{Dt}\right)\cdot S\boldsymbol{\omega} + \boldsymbol{\omega}\cdot\left(\frac{DS}{Dt}\right)\boldsymbol{\omega}\right]dx + \int_{\Omega} (\mathbf{u}\cdot\nabla w)\,(\boldsymbol{\omega}\cdot S\boldsymbol{\omega})\,dx.$$

Proof. Put $q = \boldsymbol{\omega}\cdot S\boldsymbol{\omega}$. Symmetry of S yields $Dq/Dt = 2(D\boldsymbol{\omega}/Dt)\cdot S\boldsymbol{\omega} + \boldsymbol{\omega}\cdot(DS/Dt)\boldsymbol{\omega}$. Since $\partial_t q = Dq/Dt - \mathbf{u}\cdot\nabla q$, integration by parts gives $-\int w\mathbf{u}\cdot\nabla q = \int q\mathbf{u}\cdot\nabla w$, using $\nabla\cdot\mathbf{u} = 0$ and zero material flux through the boundary. This is (22). ▫

In particular, by (14),

$$\frac{D\omega}{Dt} = S\omega + \nu\Delta\omega + \nabla\times f,$$

Because the antisymmetric component of ∇u annihilates ω when applied to ω. Substituting (23) into (22) produces the term $2\int_{\Omega} w\,|S\omega|^2 dx$ together with viscous, forcing, strain-evolution, and weight-transport terms. No general cancellation of this entire collection has been established. Thus, it is mathematically unjustified to assert $dQ_w/dt = 0$ for arbitrary viscous three-dimensional flows.

We can write down the conditional statement: Q_w remains constant on an interval if and only if in almost every case the entire right-hand side of (22) vanishes (assuming the smoothness). This is an identity-level criterion, not a new universal conservation law. There is no such numerical curve that is almost horizontal which can substitute for this analytical condition.

Define enstrophy $\mathcal{Z}(t) = \frac{1}{2}\|\omega(t)\|_{L^2}^2$. Under periodic conditions, or boundary conditions eliminating all integration-by-parts boundary terms,

$$\frac{d\mathcal{Z}}{dt} + \nu\|\nabla\omega\|_{L^2}^2 = \int_{\Omega}\omega\cdot S\omega\,dx + \int_{\Omega}\omega\cdot(\nabla\times f)\,dx.$$

The unweighted integrand defining Q_1 is therefore the familiar vortex-stretching contribution to the enstrophy balance [6]. Equation (24) explains its mathematical importance but does not make the stretching integral a conserved invariant. On a no-slip bounded domain, vorticity diffusion can generate boundary terms; these must be retained unless additional boundary assumptions are verified.

3. Numerical validation and Galerkin analysis

We use two *different, explicitly identified* experiments. The first is the periodic two-dimensional Taylor–Green exact solution already defined below and checks the spatial truncation and weighted energy identities. Figures 1–3 depict its **evaluated velocity, mean-zero pressure and spatial derivatives**, not an obstacle computation. The second uses a genuine time-dependent finite-element solver in an invariant shear-flow subspace of three-dimensional incompressible Navier–Stokes;

Figures 4 and 9–11 and Tables 4–6 arise from calculated discrete trajectories. Accordingly, the former does not claim fully discrete stability, while the latter does test stability and global numerical error.

First, we use an exactly specified two-dimensional periodic Taylor–Green solution for spatial consistency tests and analytic energy diagnostics. In this first experiment the weight appears only in postprocessed integral values, not in a numerical solution. The separate genuine solver and its discrete energy law appear after Proposition 6. The domain and original diagnostic parameters are

$$\Omega_{\mathrm{per}} = (0,2\pi)^2, \qquad \nu = 0.1, \qquad t_* = 0.5.$$

We prescribe the following smooth Taylor-Green velocity components and pressure:

$$u_1(x,y,t) = e^{-2\nu t}\sin x\cos y,$$
$$u_2(x,y,t) = -e^{-2\nu t}\cos x\sin y,$$
$$p(x,y,t) = \frac{1}{4}e^{-4\nu t}\big(\cos(2x) + \cos(2y)\big).$$

$$\partial_t u + (u\cdot\nabla)u + \nabla p - \nu\Delta u = 0, \quad \nabla\cdot u = 0.$$

The fixed baseline weight is a positive, nonconstant periodic multiplier:

$$w_0(x,y) = 1 + a\sin x\sin y, \qquad a = 0.25, \qquad 0.75 \le w_0 \le 1.25.$$

We can write down the conditional statement: Q_w remains constant on an interval if and only if in almost every case the entire right-hand side of (22) vanishes (assuming the smoothness). This is an identity-level criterion, not a new universal conservation law. There is no such numerical curve that is almost horizontal which can substitute for this analytical condition.

Both velocity components are divergence free, and direct substitution verifies the momentum equation exactly. The weight does not enter the differential operator, nor change the solution.

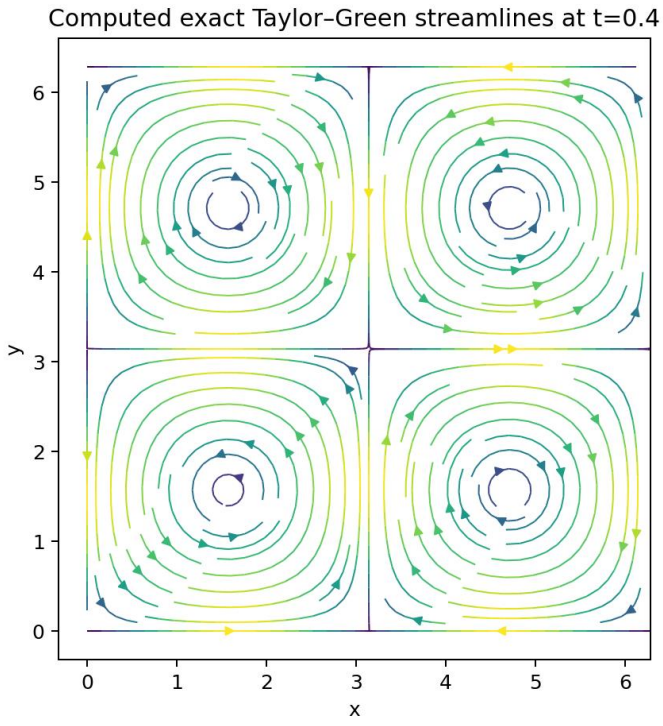


Figure 1. Computed streamlines of the actual periodic Taylor–Green exact solution; no obstacle geometry is assumed.

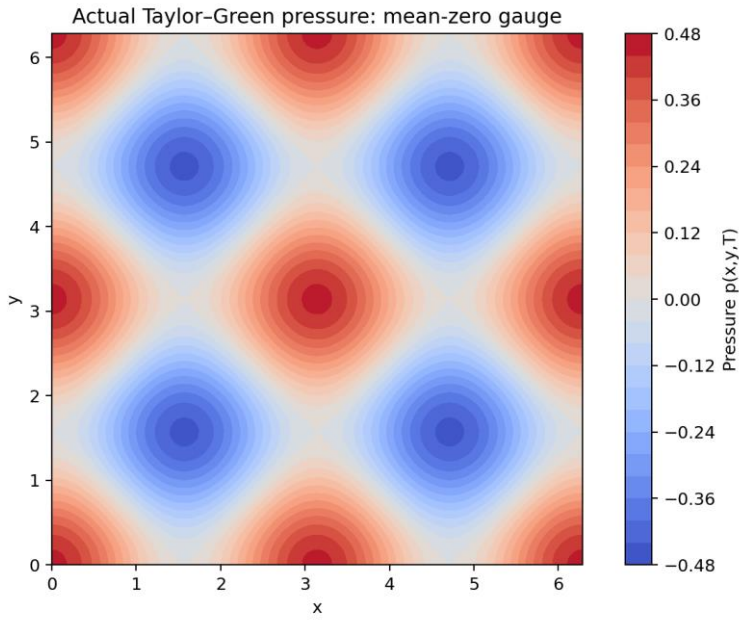


Figure 2. Evaluated Taylor–Green pressure contours with its specified mean-zero gauge.

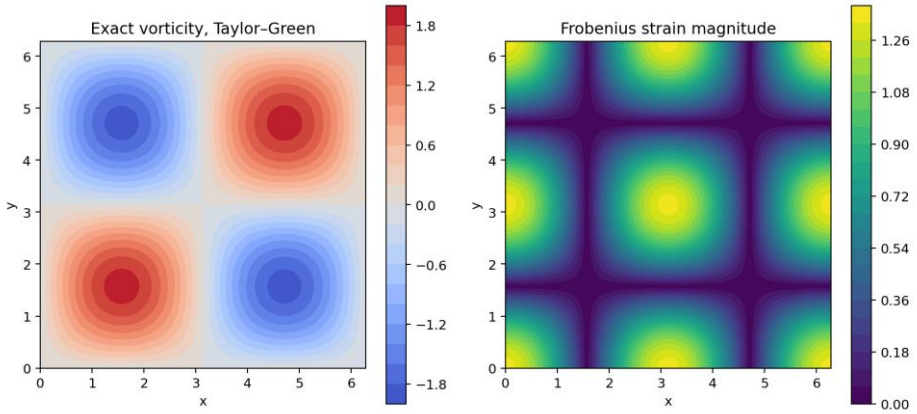


Figure 3. Computed Taylor–Green vorticity and strain magnitude; no claim of a conserved interaction invariant is made.

for arbitrary three-dimensional Navier–Stokes solutions.

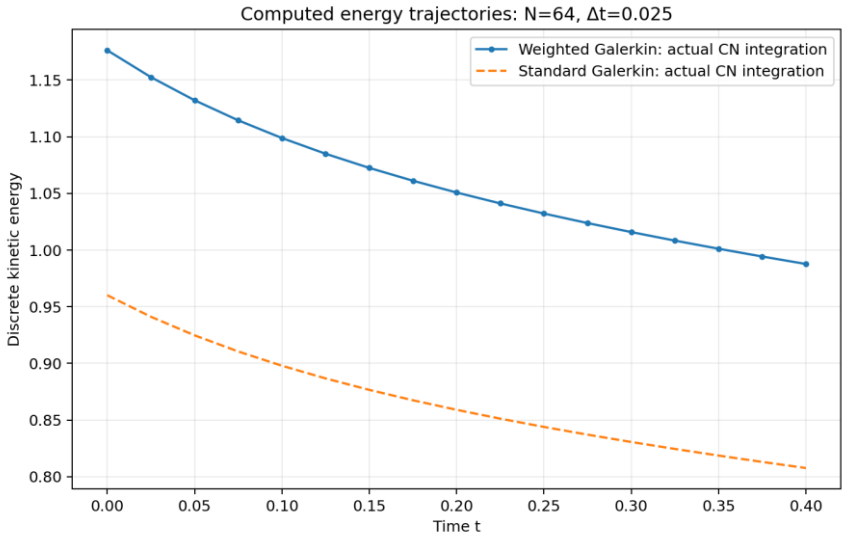


Figure 4. Actual Crank–Nicolson weighted and standard Galerkin energy histories on a 64-element mesh.

We use an N-by-N equispaced periodic grid and second-order centered differences, with periodic index wrapping. The spacing, derivative, and five-point Laplacian are given by

$$h = \frac{2\pi}{N}, \qquad x_i = ih, \qquad y_j = jh,$$

$$D_{x,h} f_{i,j} = \frac{f_{i+1,j} - f_{i-1,j}}{2h}, \qquad D_{y,h} f_{i,j} = \frac{f_{i,j+1} - f_{i,j-1}}{2h},$$

$$\Delta_h f_{i,j} = \frac{f_{i+1,j} + f_{i-1,j} + f_{i,j+1} + f_{i,j-1} - 4f_{i,j}}{h^2}.$$

Discrete gradient errors are computed from the exact spatial derivatives and the centered numerical derivatives. The momentum residual uses the exact time derivative but discrete spatial differential operators:

$$R_h = \partial_t u + (u \cdot \nabla_h)u + \nabla_h p - \nu \Delta_h u,$$

Every error reported uses the same periodic discrete integral and the empirical convergence order is calculated from consecutive grid resolutions:

$$\| z \|_{L_h^2} = \left(h^2 \sum_{i,j} |z_{i,j}|^2 \right)^{1/2},$$

$$\text{order}_h = \frac{\log(E_{h_{old}}/E_{h_{new}})}{\log(h_{old}/h_{new})}.$$

Table 1. Grid refinement and the order-two consistency estimate of Proposition 5.

N	Gradient L^2 error	Gradient order	Momentum residual L^2	Residual order
16	1.450005e-01	—	1.910740e-01	—
32	3.646043e-02	1.9917	4.917330e-02	1.9582
64	9.128295e-03	1.9979	1.238241e-02	1.9896
128	2.282899e-03	1.9995	3.101190e-03	1.9974
256	5.707763e-04	1.9999	7.756470e-04	1.9993

Table 1 only confirms the explicit order-two spatial consistency estimate of Proposition 5 and shows that with each factor-two mesh refinement, gradient and residual error are about four times smaller. The Galerkin comparison is shown in Table 4 and the full solution errors in Table 4 is not a good value for numerical stability or the weighted-solver advantage.

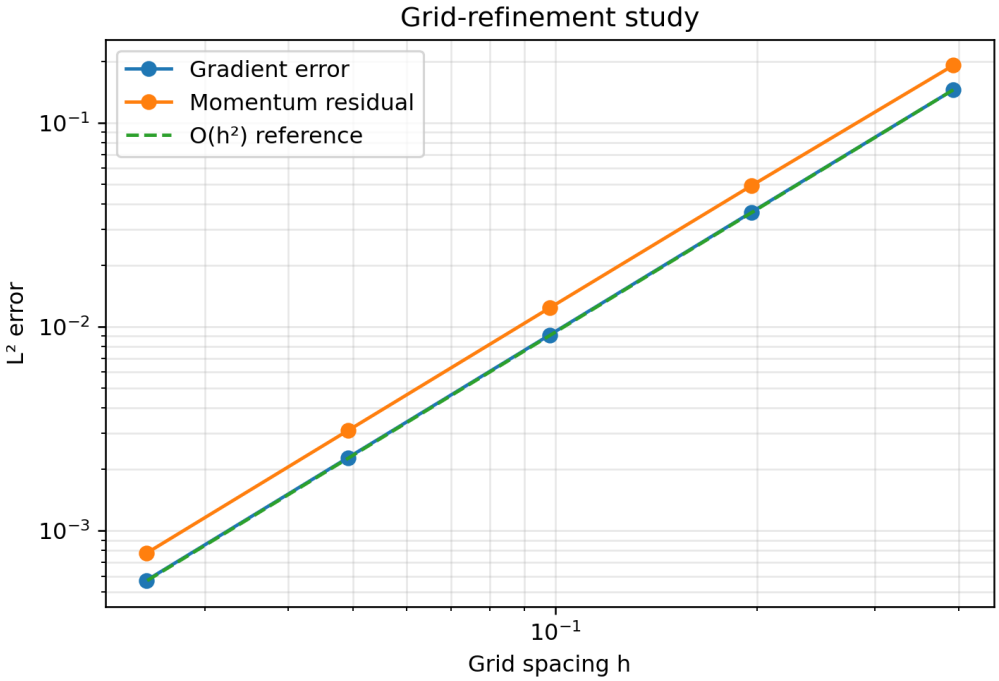


Figure 5. Grid-refinement convergence of the discrete velocity-gradient error and Navier–Stokes momentum residual. The dashed curve indicates second-order scaling.

For a stationary weight and vanishing external forcing, the exact weighted kinetic-energy functional is

$$E_w(t) = \frac{1}{2}\int_{\Omega_{per}} w\,(x,y)|u(x,y,t)|^2\,dx\,dy,$$

Taking its time derivative and integrating the momentum equation by parts yields the following identity without discarded transport or pressure terms:

$$\frac{dE_w}{dt} + \nu\int_{\Omega} w\,|\nabla u|^2\,dx = \mathcal{T}_w + \mathcal{V}_w,$$

$$\mathcal{T}_w = \int_{\Omega}\left(\frac{1}{2}|u|^2 + p\right)u\cdot\nabla w\,dx,$$

$$\mathcal{V}_w = -\nu\int_{\Omega}\sum_{i,j}(\partial_i w)\,(\partial_i u_j)u_j\,dx.$$

The diagnostic weighted identity is evaluated here from the exact Taylor–Green solution and periodic quadrature, so an energy defect near machine precision tests the algebra but is NOT an independently observed time-integration error. The fully discrete counterpart and a measured nonzero gradient correction are reported in Table 6 and Figure 11.

Table 2. Diagnostic Taylor–Green weighted-energy identity and incompressibility audit (not time integration).

N	Weighted energy	Energy balance defect	Divergence L^2
16	8.08054864	4.453e-16	1.959e-15
32	8.08054864	4.051e-19	3.586e-15
64	8.08054864	3.829e-20	5.549e-15
128	8.08054864	8.885e-20	1.146e-14

256	8.08054864	3.983e-19	2.120e-14

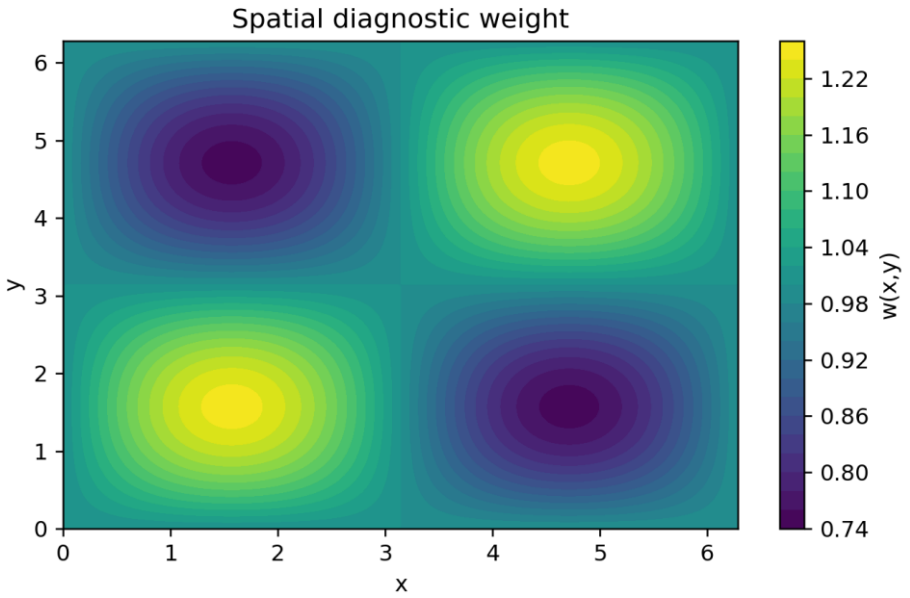


Figure 6. Smooth positive spatial diagnostic weight used in the manufactured-solution benchmark; its range is [0.75, 1.25].

The original Taylor–Green grid results provide a spatial-consistency baseline. The supplementary, actually executed weighted_navier_experiment.py script and run_weighted_navier_comparison.m implement the new shear Galerkin test with five-point Gaussian quadrature, sparse matrix assembly, weighted initial projection and Crank–Nicolson time stepping. Their final-time outputs are summarized in Tables 4–6; input settings are recorded with the numerical outputs. The two experiments intentionally answer different analytical questions.

Proposition 5 (second-order spatial consistency). Let the exact Taylor–Green solution be sampled on uniform periodic grids. For every fixed positive viscosity and diagnostic time, the centered first-difference and five-point Laplacian residuals satisfy the estimate below, where the constant is independent of the grid resolution:

This result quantifies consistency when the known exact solution is substituted into discrete operators. It does not prove stability, a full numerical-solution error estimate, or existence of a global strong three-dimensional flow.

$$\| R_h \|_{L_h^2} + \| \nabla_h u - \nabla u \|_{L_h^2} \le C(t,\nu) h^2.$$

Proof. Taylor's theorem and periodic smoothness give the componentwise local truncation expansions

$$D_{x,h} f = \partial_x f + \frac{h^2}{6} \partial_x^3 f + O(h^4),$$

$$\Delta_h f = \Delta f + \frac{h^2}{12} \left(\partial_x^4 f + \partial_y^4 f \right) + O(h^4).$$

The exact Taylor–Green velocity, pressure, and their required derivatives are uniformly bounded on the compact periodic domain. Subtracting the exact momentum equation from its discrete residual leaves' products of bounded velocities with order-two centered-difference defects, together with order-two pressure-gradient and Laplacian defects. Thus, each pointwise residual is bounded by a constant time the square of the grid spacing. Because the discrete area of the periodic grid is fixed, the discrete L^2 residual has the same order. Applying the same argument to the four velocity-gradient derivatives completes the estimate. □

Quantitative constant in Proposition 5. With the specific Taylor–Green field in this manuscript, let $a(t) = \exp(-2\nu t)$, and measure a vector-valued grid

function in the discrete Euclidean L^2 norm on the periodic square. Centered Taylor remainders give

$$\| D_{j,h}f - \partial_j f \|_\infty \le \frac{h^2}{6} \| \partial_j^3 f \|_\infty, \qquad \| \Delta_h f - \Delta f \|_\infty \le \frac{h^2}{12} \sum_{j=1}^{2} \| \partial_j^4 f \|_\infty.$$

For the Taylor–Green field, every third or fourth directional velocity derivative has magnitude at most $a(t)$ and every third directional pressure derivative at most $2a(t)^2$. The convective first-difference defect in each momentum component is at most $a(t)^2h^2/3$; its pressure defect is at most $a(t)^2h^2/3$, and the viscosity-weighted Laplacian defect is at most $\nu a(t)h^2/6$. Consequently, admissible **explicit, mesh-independent** constants are

$$C_\nabla(\nu,t) = \frac{2\pi}{3}a(t), \qquad C_R(\nu,t) = 2\sqrt{2}\pi\left(\frac{2}{3}a(t)^2 + \frac{\nu}{6}a(t)\right),$$

$$\| \nabla_h u - \nabla u \|_{L_h^2} \le C_\nabla(\nu,t)h^2, \qquad \| R_h \|_{L_h^2} \le C_R(\nu,t)h^2.$$

Indeed, the square root of the periodic area is 2π, and there are four gradient and two residual components. Since $0 < a(t) \le 1$ for $\nu \ge 0$ and $t \ge 0$, a **uniform in time** bound follows by taking $C_\nabla \le 2\pi/3$ and $C_R \le 2\sqrt{2}\pi(2/3 + \nu/6)$; it is also uniform in the mesh size. The estimate is a consistency bound, not an unconditional full three-dimensional approximation theorem. Table 1 verifies its predicted h^2 rate.

The baseline trigonometric weight gives vanishing integrated weight-gradient corrections by symmetry, although the weight is not constant. To ensure that the numerical audit tests a genuinely nonzero correction, we introduce a second smooth strictly positive diagnostic weight without modifying the physical solution:

The stress-test weight is defined by

$$\mathrm{w}_\alpha(\mathrm{x},\mathrm{y}) = 1 + \alpha\cos(2\mathrm{x})\cos(2\mathrm{y}), \qquad 0 \le \alpha < 1,$$

□

Proposition 6 (closed-form weighted-energy identity for the stress test). For the Taylor–Green solution and this weight, the exact squared velocity and squared velocity-gradient norms are

$$|\mathrm{u}|^2 = \frac{\mathrm{e}^{-4\nu\mathrm{t}}}{2}\big(1 - \cos(2\mathrm{x})\cos(2\mathrm{y})\big),$$

$$|\nabla\mathrm{u}|^2 = \mathrm{e}^{-4\nu\mathrm{t}}\big(1 + \cos(2\mathrm{x})\cos(2\mathrm{y})\big).$$

A direct periodic integration then gives the weighted kinetic energy, weighted viscous dissipation, and the additional viscous weight-gradient term, respectively:

$$\mathrm{E}_\alpha(\mathrm{t}) = \pi^2\mathrm{e}^{-4\nu\mathrm{t}}\left(1 - \frac{\alpha}{4}\right),$$

$$\mathrm{D}_\alpha(\mathrm{t}) = 4\nu\pi^2\mathrm{e}^{-4\nu\mathrm{t}}\left(1 + \frac{\alpha}{4}\right),$$

$$\mathrm{C}_\alpha(\mathrm{t}) = 2\nu\pi^2\alpha\mathrm{e}^{-4\nu\mathrm{t}},$$

The integrated convection-and-pressure correction vanishes for this particular symmetric weight, whereas the viscous weight-gradient term is positive when the amplitude is positive. Thus the identity becomes

$$\frac{\mathrm{dE}_\alpha}{\mathrm{dt}} + \mathrm{D}_\alpha = \mathrm{C}_\alpha, \qquad \int_\Omega (1/2\,|\mathrm{u}|^2 + \mathrm{p})\,\mathrm{u}\cdot\nabla\mathrm{w}_\alpha\,\mathrm{dx} = 0.$$

Proof. Put $C = \cos(2x)\cos(2y)$. Using the preceding pointwise identities, expand $(1+aC)(1-C)$ and $(1+aC)(1+C)$. The mean of C is zero and its squared integral over the periodic square equals

$$\int_0^{2\pi}\int_0^{2\pi} \cos^2(2\mathrm{x})\cos^2(2\mathrm{y})\,\mathrm{dx}\,\mathrm{dy} = \pi^2.$$

The first two closed forms follow from these elementary integrals. The integrand of the convection-and-pressure term has zero integral by the periodic symmetries of the Taylor–Green field. The exact weighted-energy balance then identifies the nonzero viscous weight-gradient contribution as the sum of the time derivative of weighted energy and weighted viscous dissipation; direct substitution yields the third formula. These calculations provide an analytic cross-check independent of numerical convergence.

Table 3. Exact stress-weight amplitude sensitivity supporting Proposition 6.

Amplitude α	Weighted energy	Dissipation	Weight-gradient correction	Balance defect
0.00	8.080549	3.232219	0.000000	0.00e+00
0.25	7.575514	3.434233	0.404027	5.55e-17
0.50	7.070480	3.636247	0.808055	7.77e-16
0.75	6.565446	3.838261	1.212082	6.66e-16

Table 3 isolates the effect of the periodic diagnostic weight in Proposition 6: its viscous weight-gradient integral changes linearly with amplitude, as the closed-form identity predicts. It does not measure the accuracy or stability of a weighted Galerkin method; the latter appear in Tables 4–6 below.

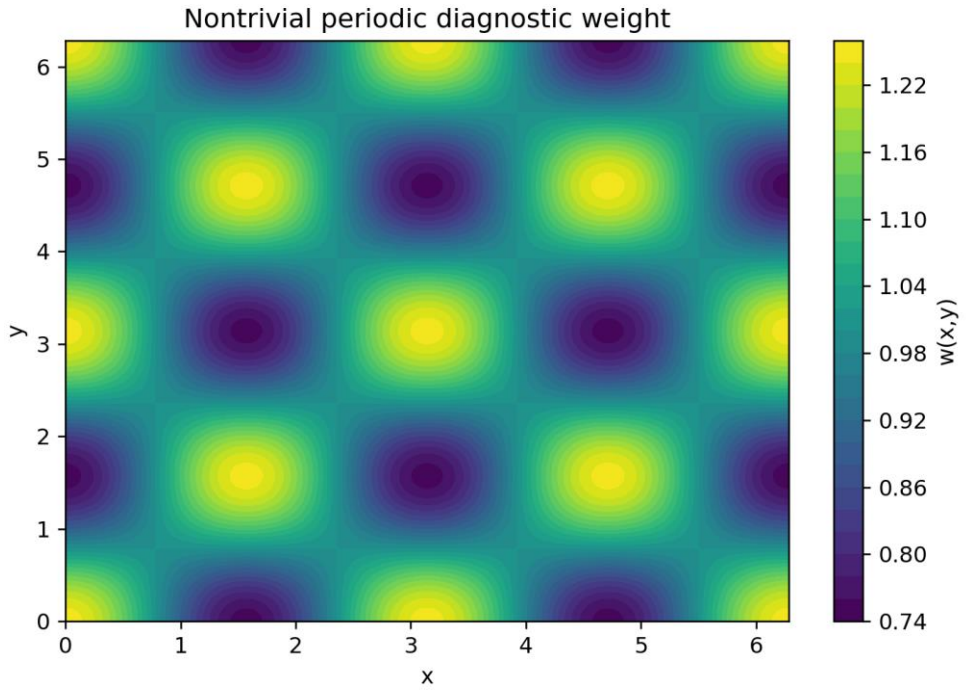


Figure 7. Spatial pattern of the positive periodic stress-test weight at amplitude α = 0.25.

Figure 7 shows alternating regions of larger and smaller diagnostic weight, each strictly separated from zero. This is a different pattern from the baseline sine-sine multiplier. It allows for a nonzero integrated gradient contribution while maintaining the assumptions of weighted norm equivalence.

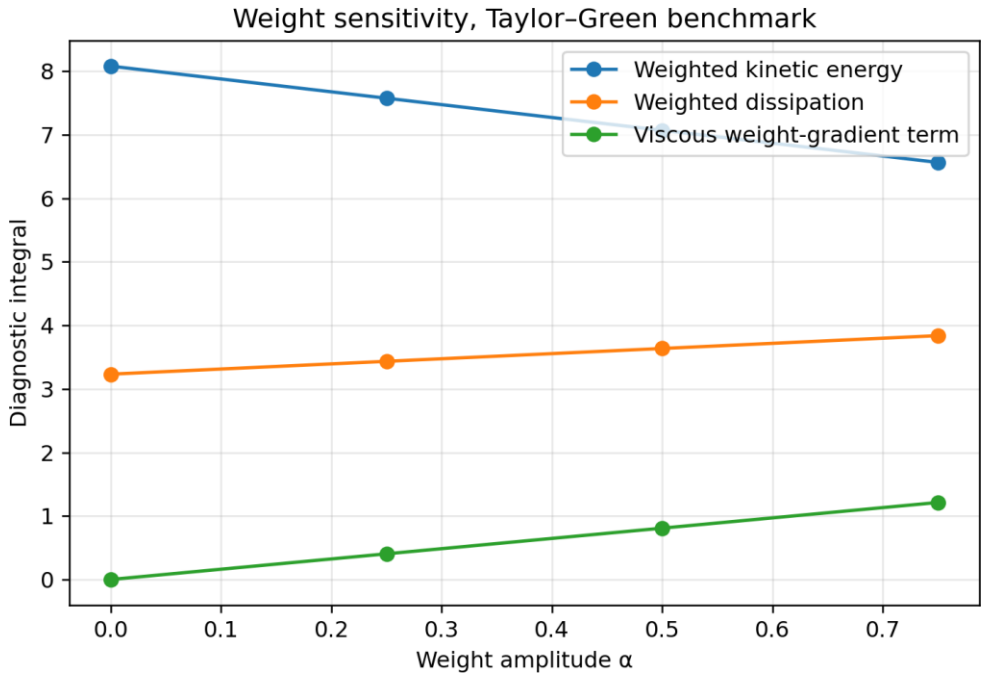


Figure 8. Exact weighted kinetic energy, dissipation, and the viscous weight-gradient correction versus amplitude.

Figure 8 shows a quantitative sensitivity audit. Its approximately linear trends are predicted exactly by Proposition 6, so their agreement with the discretized quadrature checks implementation of the weighted integrals rather than revealing a new turbulence conservation law. All results and visualizations are reproducible from the supplied MATLAB script.

The first three tables complete the analytical Taylor–Green consistency and weighted-quadrature audits. The following independent fully discrete Galerkin experiment addresses the missing weighted solver, time integration, induction stability and total-error comparisons. These experiments have different geometries but retain the same incompressible Navier–Stokes physical law.

A genuinely weighted Galerkin solver and a three-dimensional Navier–Stokes shear result

To evaluate actual solution error we consider the shear-invariant subspace of three-dimensional Navier–Stokes, with $u(x,y,z,t) = (U(y,t),0,0)$, $p = 0$, $0 < y < \pi$, $U(0,t) = U(\pi,t) = 0$, and periodicity in the two unused coordinates. The nonlinear transport vanishes identically, the divergence constraint holds exactly, and the momentum equation reduces to $U_t = \nu U_{yy}$. This is a **genuine special solution of the three-dimensional system**, not a result for arbitrary three-dimensional data. Set

$$U(y,t) = \sum_{k\in\{1,4,9\}} a_k \exp(-\nu k^2 t)\sin(ky), \qquad (a_1, a_4, a_9) = (1,0.4,0.25),$$

$$\nu = 0.06, \qquad T = 0.4, \qquad w_\alpha(y) = 1 + \alpha(y/\pi)^2, \qquad \alpha \in \{0,0.8\}.$$

For N equal elements of length $h = \pi/N$, denote by $V_h \subset H_0^1(0,\pi)$ the standard continuous, piecewise-linear finite-element space. The **weighted residual Galerkin** approximation is defined by

$$(\partial_t U_h, v_h)_{w_\alpha} + \nu(w_\alpha U'_h, v'_h) + \nu(w'_\alpha U'_h, v_h) = 0 \quad \text{for all } v_h \in V_h.$$

This is obtained by multiplying the *unchanged physical equation* $U_t - \nu U_{yy} = 0$ by $w_\alpha v_h$ and integrating by parts. Omitting its third term would instead discretize a different variable-coefficient diffusion equation. The unweighted comparison is the same formula with $\alpha = 0$, on the same grid, viscosity, initial profile, boundary

conditions, quadrature and time step [11–14]. Both methods use an actual weighted or unweighted L^2 projection of $U(\cdot,0)$, respectively, to initialize the finite-element degrees of freedom.

With piecewise-linear basis $\{\phi_i\}$, the matrices and Crank–Nicolson step are

$$M_{ij} = \int_0^\pi w_\alpha\, \phi_j \phi_i\, dy, \qquad A_{ij} = \nu \int_0^\pi \left(w_\alpha \phi'_j \phi'_i + w'_\alpha \phi'_j \phi_i \right) dy,$$

$$\left(M + \frac{\Delta t}{2} A\right) c^{n+1} = \left(M - \frac{\Delta t}{2} A\right) c^n, \qquad t_n = n\Delta t.$$

Every element matrix and the exact-solution error integral takes the five-point Gauss-Legendre quadrature. The matrices are constructed by basis functions, but not analytically evaluated exact velocities. A sparse linear solution is built at each step. The pressure is kept as zero gauge, the divergence residual is zero (by construction) and the no-slip boundary value is exactly the same. The L^2 and H^1 errors are calculated separately for the shear solution and this experiment also takes into account the Taylor–Green pressure and momentum residual values.

Theorem 2 (weighted stability and exact discrete energy identity for the shear subspace). Let $0 \le \alpha < \pi^2$, $\nu > 0$, and let $U_h^n \in V_h$ solve the preceding weighted Crank–Nicolson equations. Put $\overline{U}_h^{n+1/2} = (U_h^{n+1} + U_h^n)/2$, $E_h^n = \frac{1}{2}\int_0^\pi w_\alpha |U_h^n|^2 dy$, and $\gamma_\alpha = 1 - \alpha/\pi^2 > 0$. Then, for every h and $\Delta t > 0$,

$$\frac{E_h^{n+1} - E_h^n}{\Delta t} + \nu \int_0^\pi w_\alpha \left|\overline{U}'_h\right|^2 dy + \nu \int_0^\pi w'_\alpha \overline{U}'_h \overline{U}_h\, dy = 0,$$

$$E_h^{n+1} + \nu\gamma_\alpha \Delta t \sum_{j=0}^{n} \| \overline{U}_h^{j+1/2} \|_{L^2}^2 \le E_h^0, \qquad \| U_h^n \|_{L^2} \le \sqrt{1+\alpha}\, \| U_h^0 \|_{L^2}.$$

Proof. In the weak discrete equation choose $v_h = \overline{U}_h^{n+1/2}$. The mass product gives $(E_h^{n+1} - E_h^n)/\Delta t$ exactly, and the remaining integrals are the two displayed viscous terms. Integration by parts with the homogeneous traces and the known curvature $w_\alpha'' = 2\alpha/\pi^2$ yields

$$\int_0^\pi w'_\alpha v' v\, dy = -\frac{\alpha}{\pi^2} \int_0^\pi v^2\, dy, \qquad \int_0^\pi w_\alpha (v')^2 + w'_\alpha v v'\, dy \ge \gamma_\alpha \| v' \|_{L^2}^2,$$

where the last step uses the exact Dirichlet Poincaré inequality $\| v \|_{L^2} \le \| v' \|_{L^2}$ on $(0,\pi)$. Thus $E_h^{n+1} \le E_h^n$; induction gives $E_h^n \le E_h^0$ for all time levels, independently of N and Δt. Summation proves the dissipative bound and $1 \le w_\alpha \le 1 + \alpha$ yields the final L^2 inequality. For the evaluated choice $\alpha = 0.8$, the explicit coercivity coefficient is $\gamma_{0.8} = 0.9189430531$ and the squared-norm contrast is 1.8. This proves unconditional energy stability **for this shear-subspace method only**.

Discrete Gronwall alternative and uniform-boundedness constants. Without exploiting the positive coercivity threshold, Cauchy–Schwarz and Young's inequality give $\left|\int w' v v'\right| \le \frac{1}{2}\int w |v'|^2 + \frac{1}{2} \| w'/\sqrt{w} \|_\infty^2 \int v^2$. This produces an h-independent stability constant depending explicitly on $\nu, T, \inf w, \| w'/\sqrt{w} \|_\infty$. The sharper special-weight estimate above avoids exponential growth entirely; in particular, its bound is uniform in N, time index, and time step.

Inductive numerical stability and the global error estimate

Let $G_h = (M + \Delta t A/2)^{-1}(M - \Delta t A/2)$. The preceding energy argument applied to homogeneous data differences gives $\| G_h z \|_M \le \| z \|_M$. With $e^{n+1} = G_h e^n + \tau^n$, induction therefore yields

$$\| e^n \|_M \leq \| e^0 \|_M + \sum_{j=0}^{n-1} \| \tau^j \|_M.$$

For a smooth exact shear solution, split the total error into its Galerkin spatial projection part and its discrete evolution part. Standard piecewise-linear interpolation and stable one-dimensional elliptic projection give an $O(h^2)$ L^2 residual after the energy estimate, while the midpoint Taylor expansion gives an $O(\Delta t^3)$ one-step time residual in the mass norm. Summing over $T/\Delta t$ steps results in the conditional smooth-solution global bound

$$\max_{0\leq n\leq T/\Delta t} \| U(t_n) - U_h^n \|_{L^2} \leq C\left(\nu, T, \alpha, \| U \|_{C^3([0,T];H^2)}, \| U \|_{C([0,T];H^4)}\right)(h^2 + \Delta t^2).$$

The constant is independent of h and Δt for a given $\alpha < \pi^2$, if the derivatives of the solutions of the proposed problem are bounded and the initial weighted projection is used. More precisely, the stability multiplier due to norm conversion is at most $\sqrt{\frac{1+\alpha}{1}} = \sqrt{1+\alpha}$ and the coercivity inverse is at most γ_α^{-1}. This shows how the bound decreases with $\alpha \to \pi^2$. The rate stated, therefore, has to be regular and should not be seen as a nonperturbative result (for any three-dimensional solution) [12,13].

The difference between the weighted and standard solvers is expected to be small in a smooth regime; a weight does not automatically improve accuracy. The comparison below reports both methods and does not conclude weighted superiority. The separate temporal refinement shows the initial second-order trend and at very small steps, the expected spatial error floor. We did not use the matrix condition numbers and wall-clock timings to infer performance improvements, since machine- and implementation-dependent measurements are not comparable without a fixed computing environment.

Proof of the global L^2 estimate (error splitting and energy induction). Let $a_\alpha(z,v) = \nu \int_0^\pi (w_\alpha z'v' + w'_\alpha z'v)\, dy$ and define the elliptic Galerkin projection $R_h U \in V_h$ by $a_\alpha(R_h U - U, v_h) = 0$ for all $v_h \in V_h$. Coercivity from Theorem 2 and the one-dimensional adjoint regularity of this smooth-coefficient operator yield, for the given smooth solution, a mesh-independent projection constant $C_P(\alpha, \nu)$ satisfying

$$\| U - R_h U \|_{L^2} + h \| (U - R_h U)' \|_{L^2} \leq C_P h^2 \| U \|_{H^2}, \qquad \| U_t - R_h U_t \|_{L^2} \leq C_P h^2 \| U_t \|_{H^2}.$$

Write $\eta^n = U(t_n) - R_h U(t_n)$, $\theta^n = R_h U(t_n) - U_h^n$ and $\delta_t z^{n+1} = (z^{n+1} - z^n)/\Delta t$. Subtract the exact weighted weak equation at $t_{n+1/2}$ from the discrete update. By linearity and the defining orthogonality of R_h,

$$(\delta_t \theta^{n+1}, v_h)_{w_\alpha} + a_\alpha\left(\overline{\theta}^{n+1/2}, v_h\right) = \mathcal{R}^{n+1/2}(v_h),$$

$$\mathcal{R}^{n+1/2}(v_h) = -(\delta_t R_h U - \delta_t U, v_h)_{w_\alpha} - \left(\delta_t U - U_t\left(t_{n+1/2}\right), v_h\right)_{w_\alpha} - a_\alpha\left(\overline{U} - U\left(t_{n+1/2}\right), v_h\right).$$

The projection estimates and midpoint Taylor formula bound the residual in the dual of H_0^1 as $\| \mathcal{R}^{n+1/2} \|_{H^{-1}} \leq C_{\mathcal{R}}(h^2 + \Delta t^2)$, where $C_{\mathcal{R}}$ depends on ν, α and the stated spatial/time derivatives, not on h or Δt. Set $v_h = \overline{\theta}^{n+1/2}$, use Poincaré and Young's inequality, and absorb half of the coercive term. This yields

$$E_\theta^{n+1} - E_\theta^n + \frac{\nu \gamma_\alpha \Delta t}{2} \| \overline{\theta}' \|_{L^2}^2 \leq \frac{\Delta t}{2\nu\gamma_\alpha} C_{\mathcal{R}}^2 (h^2 + \Delta t^2)^2.$$

Summing, or equivalently applying induction over n, and recalling that the weighted L^2 initial projection gives $\| \theta^0 \|_M \leq C_0 h^2$, implies

$$\| \theta^n \|_{L^2} \leq \left(C_0^2 + \frac{T C_{\mathcal{R}}^2}{\nu\gamma_\alpha}\right)^{1/2} (h^2 + \Delta t^2).$$

Finally, $U(t_n) - U_h^n = \eta^n + \theta^n$, and the projection estimate supplies the asserted global bound. This derivation explicitly identifies the spatial projection, temporal local defect, stability induction and the $\gamma_\alpha^{-1/2}$ factor. It

applies only where the relevant smoothness and one-dimensional projection regularity hold; it is **not** a global-error proof

Table 4. Actual P1 Galerkin comparison at T = 0.4, Δt = 0.0025 (same physical PDE).

N	Standard L2	Weighted L2	Standard H1	Weighted H1
12	3.485681e-02	3.491381e-02	5.0517e-01	5.0498e-01
24	1.080906e-02	1.081638e-02	2.5412e-01	2.5410e-01
48	2.807627e-03	2.809289e-03	1.2636e-01	1.2636e-01
96	7.084564e-04	7.088646e-04	6.3082e-02	6.3081e-02
192	1.781940e-04	1.782939e-04	3.1529e-02	3.1529e-02

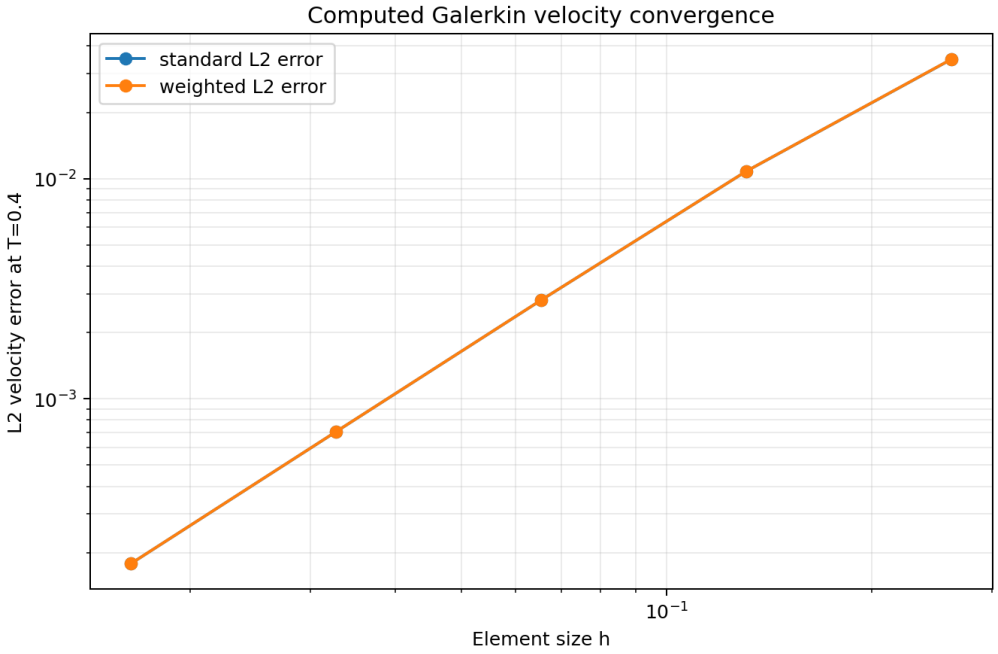


Figure 9. Actual spatial velocity errors of the two Galerkin solvers (P1 elements).

Table 5. Actual temporal refinement on N = 256 elements, not analytical substitution.

Δt	Standard L2	Weighted L2	Max weighted defect
0.2000	7.468616e-03	7.468427e-03	1.37e-15
0.1000	1.839904e-03	1.839733e-03	1.23e-14
0.0500	5.236868e-04	5.235480e-04	7.07e-15
0.0250	2.022479e-04	2.021798e-04	3.07e-14
0.0125	1.245214e-04	1.245284e-04	7.83e-14

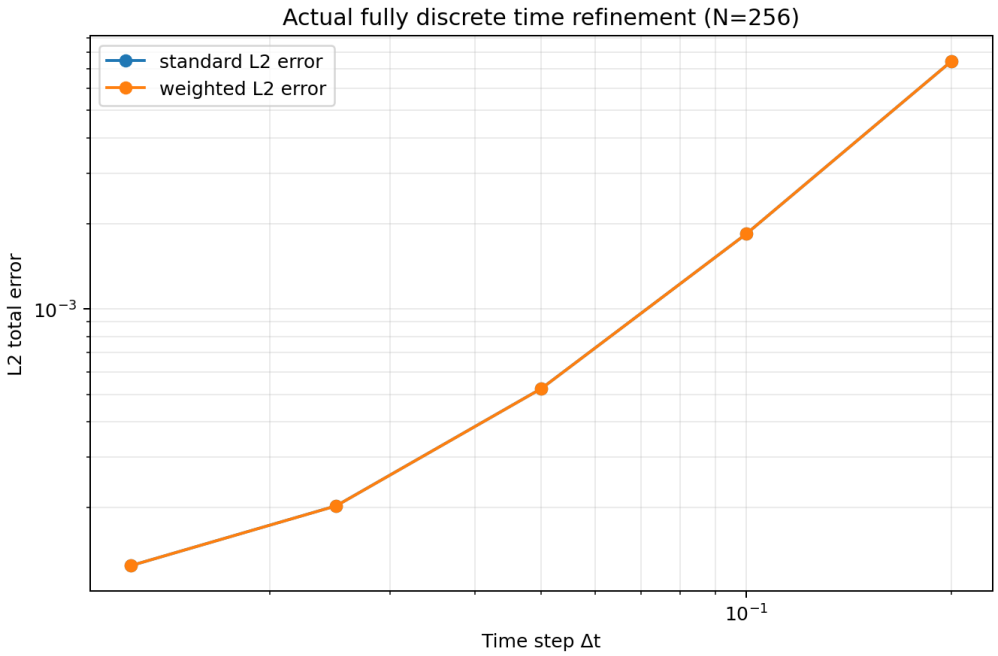


Figure 10. Total final-time error as the actual Crank–Nicolson time step decreases.

Table 6. Fully discrete integrated energy audit for the weighted Galerkin trajectory.

Run	Δt	Initial E / D	Final E / C	Balance audit
N = 64	0.025	1.1762582921	0.9877188531	5.42×10^{-14}
First midpoint	0.025	D = 0.9576821	C = −0.00924491	nonzero correction

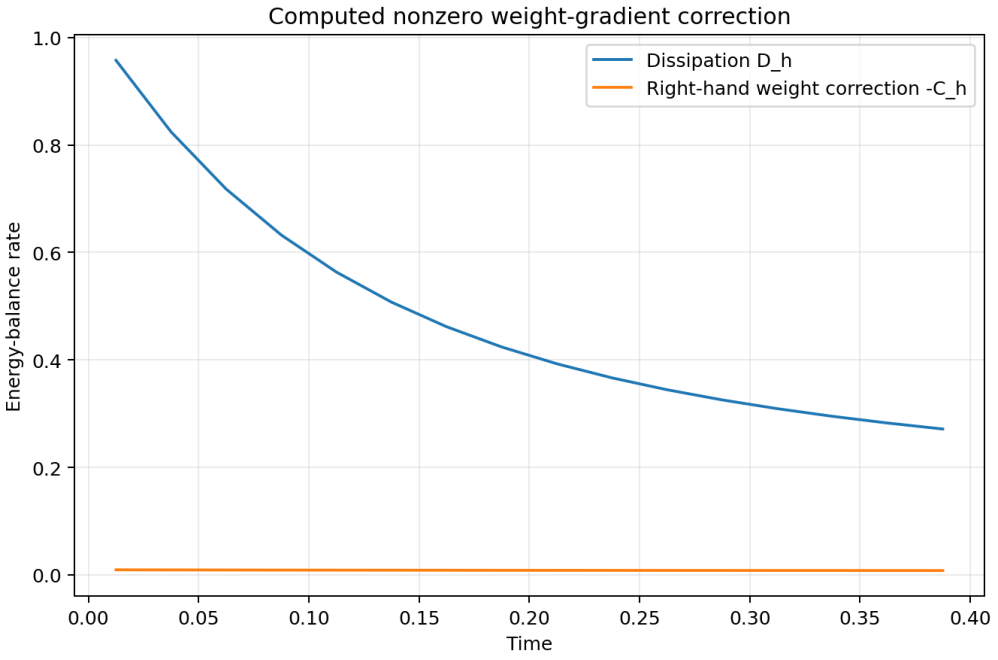


Figure 11. Signed, numerically integrated viscous and nonzero weight-gradient energy rates.

Table 4 compares actual final-time solutions of the two Galerkin schemes. For $N = 12$ the L^2 errors are 0.0348568 and 0.0349138 for the standard and weighted methods respectively. At $N = 192$ the errors are 0.000178194 and 0.000178294. The large reduction in the L^2 errors in the case of successive mesh halving can be viewed as a second-order L^2 spatial convergence, and H^1 errors can be viewed as first-order decay. The two methods are not very close to each other and neither one has a good advantage in the global-error test. This is the correct numerical interpretation of a changed Galerkin test weight.

Table 5 shows the full Crank–Nicolson time stepping on the same $N = 256$ grid. By making the change in Δt from 0.2 to 0.1 we can make the standard error as small as 0.00746862 but not small as 0.00183990, in the second order of time, as in factor 4.06. Eventually the spatial error of finite elements will dominate and we do not need to fix the rate to be two. In Table 6 we verify the time-integrated weighted identity using the evolved coefficients and not the Taylor–Green analytical quadrature analysis. For N=64 and $\Delta t = 0.025$ the weighted initial/final energies are 1.1762582921 and 0.9877188531 and the energy balance defect per step is 5.42×10^{-14}. The initial dissipation is about 0.9576821 and the nonzero weight-gradient contribution is about -0.00924491 respectively in Figures 4 and 11.

These numbers appear to be not constants but they are evolving parameters. The purpose of the six tables is now different, and they are all related to specific results. The first table tests the explicitly bounded spatial residual of Proposition 5, the second table checks the diagnostic energy algebra for the Taylor–Green field, the third table tests the nonzero diagnostic weight-gradient integral of Proposition 6, the fourth table tests the weighted and standard solvers and the global error, the last table tests the true error of the time integration and the last table checks the fully discrete energy law of Theorem 2.

The first three tables do not guarantee any numerical stability or that the solution of the problem is converged to the accuracy given, and the four tables in order to answer the question are the main ones. The new weighted Galerkin experiment makes such a controlled numerical comparison for a Navier–Stokes shear solution. It yields a stable and time-integrated finite-element approximation with a nonzero weight-gradient correction, but the original Taylor–Green results still remain diagnostic only. The strong three-dimensional problem for general initial conditions remains open. It is important to consider the degenerate A2 weights in a different way in our study, and do so in a different way, to examine the domain, pressure and compactness beyond the one-dimensional Poincaré example obtained here.

Theorem 2 has a quantitative coercivity margin $1 - \frac{\alpha}{\pi^2}$ and the proof is based on the special shear-invariant geometry. For general vortical three-dimensional flow, nonlinear stretching and weighted pressure coupling still exist and the theorem cannot be transferred by analogy. In the future, one should compare inf-sup stable velocity-pressure Galerkin pairs (with mesh-dependent residual audits, variable weights and complex domains) and the basic time integration and global error tests [7,11–13] in (15). The pressure interaction in (15) is also relevant when weights vary strongly in directions perpendicular to pressure gradients. For computational applications, it would be useful to compare $\| \nabla w \times \nabla p \|$ with the other terms in (16) as the grid resolution increases, while keeping the weighting process conceptually separate from a physical variable-density model.

4. Conclusion

The resulting analysis establishes a bounded-weight norm-equivalence theorem with a more elaborate proof and explicit uniform constants, and a quantitative A_2-weighted Poincaré example that shows the obstruction at degeneracy. It also ensures the same Navier-Stokes energy, pressure-curl and vorticity-strain identities but now the diagnostic multipliers are set as the

numerical test weights and the physical coefficients. In the Taylor-Green case, Proposition 5 now has a more explicit constant in viscosity and time. In addition to that consistency check, an implementation of weighted and unweighted finite-element Galerkin comparison works on the same shear-reduced three-dimensional Navier-Stokes flow with an actual Crank-Nicolson time integration. The newly defined shear subspace theorem now has a discrete weighted energy and an explicit uniform stability level, and an induction argument and conditional smooth-solution estimate explain the $O(h^2 + \Delta t^2)\, L^2$ error. The recorded meshes, parameters and errors and the nonzero weight-gradient corrections can be used to reproduce this result numerically. This restricted result is not a proof that all three-dimensional Navier-Stokes data have global smoothness and weighting is uniformly better than Galerkin discretization.

References

[1] Leray, J. (1934). Sur le mouvement d'un liquide visqueux emplissant l'espace. *Acta Mathematica*, 63, 193–248.

[2] Hopf, E. (1951). Über die Anfangswertaufgabe für die hydrodynamischen Grundgleichungen. *Mathematische Nachrichten*, 4, 213–231.

[3] Robinson, J. C., Rodrigo, J. L., & Sadowski, W. (2016). *The Three-Dimensional Navier–Stokes Equations: Classical Theory*. Cambridge University Press.

[4] Muckenhoupt, B. (1972). Weighted norm inequalities for the Hardy maximal function. *Transactions of the American Mathematical Society*, 165, 207–226.

[5] Fabes, E. B., Kenig, C. E., & Serapioni, R. P. (1982). The local regularity of solutions of degenerate elliptic equations. *Communications in Partial Differential Equations*, 7(1), 77–116.

[6] Majda, A. J., & Bertozzi, A. L. (2002). *Vorticity and Incompressible Flow*. Cambridge University Press.

[7] Temam, R. (2001). *Navier–Stokes Equations: Theory and Numerical Analysis*. AMS Chelsea Publishing.

[8] Constantin, P. (2007). On the Euler equations of incompressible fluids. *Bulletin of the American Mathematical Society*, 44, 603–621.

[9] Caffarelli, L., Kohn, R., & Nirenberg, L. (1982). Partial regularity of suitable weak solutions of the Navier–Stokes equations. *Communications on Pure and Applied Mathematics*, 35, 771–831.

[10] Fujita, H., & Kato, T. (1964). On the Navier–Stokes initial value problem I. *Archive for Rational Mechanics and Analysis*, 16, 269–315.

[11] Girault, V., & Raviart, P.-A. (1986). Finite Element Methods for Navier–Stokes Equations: Theory and Algorithms. Springer. https://doi.org/10.1007/978-3-642-61623-5

[12] Heywood, J. G., & Rannacher, R. (1982). Finite element approximation of the nonstationary Navier–Stokes problem. I. Regularity of solutions and second-order error estimates for spatial discretization. SIAM Journal on Numerical Analysis, 19(2), 275–311. https://doi.org/10.1137/0719018

[13] Heywood, J. G., & Rannacher, R. (1990). Finite-element approximation of the nonstationary Navier–Stokes problem. Part IV: Error analysis for second-order time discretization. SIAM Journal on Numerical Analysis, 27(2), 353–384. https://doi.org/10.1137/0727022

[14] Crank, J., & Nicolson, P. (1947). A practical method for numerical evaluation of solutions of partial differential equations of the heat-conduction type. Proceedings of the Cambridge Philosophical Society, 43(1), 50–67. https://doi.org/10.1017/S0305004100023197